THE JOURNAL OF BIOLOGICAL CHEMISTRY VOL. 283, NO. 22, pp. 15460–15468, May 30, 2008
Printed in the U.S.A.

A Threonine on the Active Site Loop Controls Transition State Formation in *Escherichia coli* Respiratory Complex II*[S]

Received for publication, February 20, 2008, and in revised form, March 26, 2008 Published, JBC Papers in Press, April 2, 2008, DOI 10.1074/jbc.M801372200

Thomas M. Tomasiak[‡], Elena Maklashina[§¶], Gary Cecchini[§¶1], and Tina M. Iverson[‡‖2]

From the Departments of [‡]Pharmacology and [‖]Biochemistry, Vanderbilt University, Nashville, Tennessee 37232, the [§]Molecular Biology Division, Veterans Affairs Medical Center, San Francisco, California 94121, and the [¶]Department of Biochemistry and Biophysics, University of California, San Francisco, California 94158

In *Escherichia coli*, the complex II superfamily members succinate:ubiquinone oxidoreductase (SQR) and quinol:fumarate reductase (QFR) participate in aerobic and anaerobic respiration, respectively. Complex II enzymes catalyze succinate and fumarate interconversion at the interface of two domains of the soluble flavoprotein subunit, the FAD binding domain and the capping domain. An 11-amino acid loop in the capping domain (Thr-A234 to Thr-A244 in quinol:fumarate reductase) begins at the interdomain hinge and covers the active site. Amino acids of this loop interact with both the substrate and a proton shuttle, potentially coordinating substrate binding and the proton shuttle protonation state. To assess the loop's role in catalysis, two threonine residues were mutated to alanine: QFR Thr-A244 (act-T; Thr-A254 in SQR), which hydrogen-bonds to the substrate at the active site, and QFR Thr-A234 (hinge-T; Thr-A244 in SQR), which is located at the hinge and hydrogen-bonds the proton shuttle. Both mutations impair catalysis and decrease substrate binding. The crystal structure of the hinge-T mutation reveals a reorientation between the FAD-binding and capping domains that accompanies proton shuttle alteration. Taken together, hydrogen bonding from act-T to substrate may coordinate with interdomain motions to twist the double bond of fumarate and introduce the strain important for attaining the transition state.

Complex II superfamily members catalyze two distinct chemical reactions: the interconversion of succinate and fumarate and the interconversion of quinone and quinol (1). In this capacity, complex II links the citric acid cycle to the electron transfer chain. The two reactions are coupled, since electrons that are the product of one reaction are transferred through the complex II enzyme to become the reactant of the second reaction. Homologues of complex II that preferentially oxidize succinate and reduce quinone participate in aerobic respiration are known as succinate:ubiquinone oxidoreductases (SQR[3]; SdhCDAB). By contrast, those homologues that preferentially reduce fumarate and oxidize quinol are known as quinol:fumarate reductases (QFR; FrdABCD) and participate in bacterial anaerobic respiration with fumarate as the terminal electron acceptor.

Complex II enzymes contain four polypeptide chains, two of which, the flavoprotein (FrdA; SdhA) and the iron protein (FrdB; SdhB), are soluble subunits and two of which span the membrane (FrdCD; SdhCD) (2). Succinate and fumarate interconversion occurs in the flavoprotein, whereas quinol and quinone interconversion occurs in the membrane-spanning region of the protein. In addition to the integral-membrane complex II homologues, there are known soluble homologues of the flavoprotein that only catalyze dicarboxylate oxidoreduction without coupling this reaction to quinone chemistry within the membrane.

Both the soluble and integral membrane homologues of complex II contain an FAD prosthetic group in the flavoprotein that performs hydride transfer during catalysis. In the membrane-bound forms of complex II, covalent binding of FAD raises its potential (E_{m7} = ~−55 to −70 mV) and allows membrane-bound enzymes to proficiently oxidize succinate as well as reduce fumarate (3–6). In contrast, noncovalently bound FAD in the soluble bacterial homologues, such as flavocytochrome c_3 (Fcc_3) and L-aspartate oxidase, has a redox potential ~100 mV lower (~−150 mV) (7). As a result, these soluble homologues cannot proficiently oxidize succinate (8–11).

X-ray structures from the complex II superfamily reveal that the active site for dicarboxylate oxidoreduction shares a common architecture with absolutely conserved catalytic residues (1, 2, 8–17). Like its eukaryotic and prokaryotic counterparts, the flavoprotein subunit of *Escherichia coli* SQR and QFR comprises two domains (*i.e.* an FAD-binding domain and a capping domain) with the active site at the domain interface. A short

* This work was supported, in whole or in part, by National Institutes of Health Grants GM61606 (to G. C.), GM079419 (T. M. I.), and T32 GM65086 (to T. T.) and a pilot award funded by Grant P30 ES000267 (to T. M. I.). This work was also supported by the Department of Veterans Affairs and Ellison Medical Foundation Grant AG-NS-0325 (to T. M. I.). The costs of publication of this article were defrayed in part by the payment of page charges. This article must therefore be hereby marked "*advertisement*" in accordance with 18 U.S.C. Section 1734 solely to indicate this fact.

The atomic coordinates and structure factors (code 3CIR) have been deposited in the Protein Data Bank, Research Collaboratory for Structural Bioinformatics, Rutgers University, New Brunswick, NJ (http://www.rcsb.org/).

[S] The on-line version of this article (available at http://www.jbc.org) contains supplemental Fig. S1.

[1] To whom correspondence may be addressed: Molecular Biology Division, Veterans Affairs Medical Center, San Francisco, CA 94121. Tel.: 415-221-4810 (ext. 4416); E-mail: gary.cecchini@ucsf.edu.

[2] To whom correspondence may be addressed: Dept. of Pharmacology, Vanderbilt University, 460 Robinson Research Bldg., Nashville, TN 37232-6600. Tel.: 615-322-7817; Fax: 615-343-6532; E-mail: tina.iverson@vanderbilt.edu.

[3] The abbreviations used are: SQR, succinate:ubiquinone oxidoreductase; QFR, quinol:fumarate reductase; CT, charge transfer; OAA, oxaloacetate; act-T, FrdA T244A or SdhA T254A mutation; hinge-T, FrdA T234A or SdhA T244A mutation; BisTris, 2-[bis(2-hydroxyethyl)amino]-2-(hydroxymethyl) propane-1,3-diol; Fcc_3, flavocytochrome c_3.

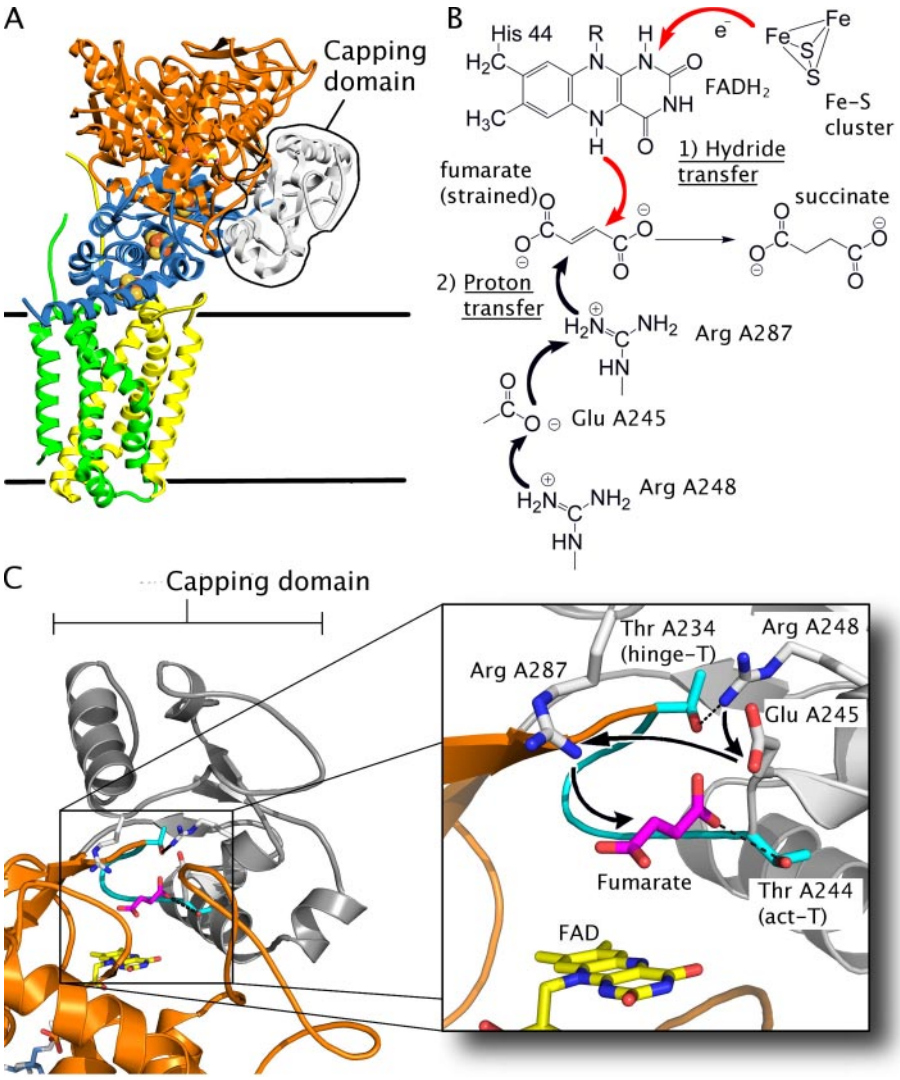

FIGURE 1. **Overview of active site architecture and the fumarate reduction reaction mechanism in complex II enzymes.** *A*, the overall architecture of wild type *E. coli* QFR (Protein Data Bank code 1KF6) is shown in relation to the membrane. The FrdA subunit (*orange*) is shown with the capping domain (*gray*) *circled*. The FrdB (*blue*), FrdC (*yellow*), and FrdD (*green*) subunits are shown as *ribbons*, with iron-sulfur clusters of the FrdB subunit shown as *spheres*. *B*, in QFR and soluble fumarate reductases, fumarate reduction is believed to occur in two distinct steps. The first is hydride transfer from reduced FAD, and the second is proton transfer from Arg-A287. Electron transfer and hydride transfer are displayed as *red arrows*, and all proton transfer steps are shown with *black arrows*. Reprotonation of the Arg-A287 side chain is achieved through a shuttle comprising Glu-A245 and Arg-A248. Although rereduction of the FAD requires two electrons that are transferred from iron-sulfur clusters in the iron protein subunit protein, the pathway for reprotonation of the FAD has not been elucidated. *C*, the QFR active site is located in the flavoprotein (FrdA) at the interface between the FAD binding domain (*orange*) and the capping domain (*gray*). The active site loop (*cyan*) contains both proton shuttling residues and substrate binding residues. Nitrogen atoms are colored *blue*, oxygen is colored *red*, FAD carbons are *yellow*, and fumarate carbons are *magenta*. Side chain carbons are colored *gray* for Arg-A245, Arg-A248, and Arg-A287; side chain carbons for act-T and hinge-T are colored *cyan*. The location of fumarate in the active site is from an unpublished structure and matches published Fcc_3 (Protein Data Bank code 1D4E) (11) and *W. succinogenes* (Protein Data Bank code 1QLB) (21) co-structures. The *black arrows* indicate the direction of proton transfer through the proton shuttle during fumarate reduction.

hinge region connects these two domains (Fig. 1*A*; residues 231–234 and 351–353 of the QFR flavoprotein subunit). The FAD-binding and capping domains can assume any of a continuum of interdomain angles without distortion of the fold of either domain (2, 8–11, 18–23). These flavoprotein structures can be categorized into three groups, depending on interdomain orientation (19): domains "closed" over the active site (16, 18, 19, 22), domains rotated into an "open" position for solvent access into the active site (8, 9), and an "intermediate" position (10, 11, 20, 21, 23). Although all of the structures in the open state lack bound dicarboxylate at the active site (8, 9), there has also been a structure of a dicarboxylate-free active site in the closed position (16). In general, the majority of structures with ligand bound into the active site are in closed or intermediate positions that are nearly closed. The flavoproteins of both the *Wolinella succinogenes* QFR (20, 22) and the soluble Fcc_3 flavoproteins (9, 10) have been observed with different domain angles in different crystal forms, suggesting that crystal packing forces can alter the interdomain angle and reflect the flexibility between these domains. The physiological significance of interdomain flexibility in the complex II superfamily is debated (24), and there is currently no known correlation between domain rotations and the catalysis. However, this type of interdomain movement has been suggested to control substrate access to the active site in a number of other flavoenzymes (25).

Intriguingly, the interdomain hinge between the FAD-binding and capping domains contains an absolutely conserved His-Pro-Thr motif that begins in an 11-amino acid loop (Fig. 2*A*) containing residues important for catalysis in QFR and SQR (Fig. 1*B*). This active site loop begins at the hinge with a threonine (Thr-A234 in the *E. coli* QFR, Thr-A244 in the *E. coli* SQR) denoted as the hinge-T. The loop ends at a second threonine (Thr-A244 in *E. coli* QFR, Thr-A254 in the *E. coli* SQR) that forms a hydrogen-bonding interaction to the substrate in the active site and is denoted as act-T.

The act-T hydrogen bond to substrate is particularly notable, since it may prime fumarate to accept hydride transfer from FAD, the first step in fumarate reduction by QFR. In solution, fumarate is a planar molecule constrained by a double bond (12); however, in complex II co-structures with fumarate, the O1 and O2 oxygen atoms are out of plane with the rest of the molecule (11, 20). The strain across the double bond of fumarate may facilitate hydride transfer from flavin N5 to fumarate C2 by stabilizing the transition state and lowering the transition state barrier (11, 12).

The second step of fumarate reduction in QFR, protonation of the intermediate carbanion, may be influenced by hinge-T (QFR Thr-A234), located at the end of the interdomain hinge and the beginning of the active site loop. The hinge-T side chain Oγ forms a hydrogen-bonding interaction with the side chain guanidino Nζ atom of Arg 248, which is a part of the proton shuttle that delivers a proton to the buried active site. This proton shuttle begins with Arg-A248, extends through Glu-A245, and ends with Arg-A287, which directly interacts with substrate (12, 26–29). In theory, the hydrogen-bonding interaction between the hinge-T Oγ and Arg-248 Nζ should lower the pK_a of the arginine side chain and allow proton transfer at physiological pH values.

To further investigate the unique role of the active site loop in catalysis, the function of act-T (QFR Thr-A244; SQR Thr-A254) and hinge-T (QFR Thr-A234; SQR Thr-A244) was examined using alanine mutations in the *E. coli* QFR and SQR enzymes. Both mutants showed a loss of substrate binding and a loss of catalysis. Since the hinge-T does not interact directly with substrate, the basis for the loss of substrate binding in the hinge-T mutant QFR was evaluated using x-ray crystallography, which revealed that the absence of interpretable density for bound dicarboxylate resulted from a domain reorientation. The role of the hydrogen bonds provided by act-T and hinge-T are discussed for QFR and SQR, respectively.

EXPERIMENTAL PROCEDURES

Bacterial Strains and Plasmids—*E. coli* strain DW35 (Δ*frdABCD*, *sdhC*::*kan*), which was used as the host for expression of wild type and mutant forms of QFR and SQR, has been previously described (30). Plasmid pH3 ($frdA^+B^+C^+D^+$) was used for expression of wild type QFR (4), and plasmid pFAS ($P_{FRD}sdhC^+D^+A^+B^+$) was used for expression of wild type SQR (31).

Mutagenesis—Mutation of individual amino acids was accomplished using the QuikChange (Stratagene, La Jolla, CA) site-directed mutagenesis kit. All mutations were verified by sequencing the HindIII-BstXI restriction fragment for SdhA mutations or the BstEII-ApaI fragment from FrdA. Mutagenized fragments were subcloned back into pFAS for SQR mutants or pH3 for QFR mutants. All cloning procedures were performed in accordance with methods previously described (4, 30, 31).

Growth Conditions and Enzyme Purification—*E. coli* DW35 harboring the appropriate plasmid was grown under microaerophilic conditions in Terrific Broth medium as previously described (32). Isolation of membrane fractions (33) and subsequent purification of QFR and SQR enzymes were performed according to previously published methods (31, 34). Protein concentration was measured by the bicinchoninic acid method (Pierce) with bovine serum albumin as a standard. FAD and heme content were determined as previously described (32).

Measurement of Enzyme Activity—To activate the enzymes, QFR and SQR were diluted to 5 mg of protein/ml in 30 mM BTP (BisTris-propane, pH 7.0), 0.1 mM EDTA, 0.05% Anapoe® $C_{12}E_9$ (Anatrace, Maumee, OH), 3 mM malonate and incubated for 20 min at 30 °C. For spectroscopic analysis, the enzymes were then concentrated with a Centriprep YM30 (Millipore) centrifugal filter device following the manufacturer's instructions and then passed through a PD-10 gel filtration column to remove malonate. Activated enzyme was then stored on ice for the duration of the experiment. The standard assay medium at 30 °C contained 50 mM BTP, 0.1 mM EDTA, 0.006% $C_{12}E_9$ with the pH adjusted to intervals of 6.0–9.4 as appropriate. Potassium ferricyanide and phenazine ethosulfate/2,6-dichlorophenol indophenol were used as electron acceptors for reactions of succinate oxidation for QFR and SQR, respectively (35). Fumarate reduction was determined with reduced methyl viologen or by menaquinol oxidation, as described previously (36). Optical spectra were recorded with an Agilent 8453 diode array spectrophotometer 1 min after the addition of ligand to an isolated enzyme in 30 mM BTP, 0.1 mM EDTA, 0.01% Anapoe $C_{12}E_9$.

TABLE 1
Crystallographic data collection, processing, and refinement

Parameters	Values
Wavelength (Å)	1.0
Resolution (Å)	3.65
Unit cell dimensions (Å)	$a = 96.9$, $b = 135.5$, $c = 266.0$
Space group	$P2_12_12_1$
Observations	76,015
Unique observations	32,532
I/σ	9.52 (2.5)
Completeness	80.7%
R_{sym} [a]	8.4% (39%)
R_{work} [b]	26.05%
R_{free} [c]	29.57%
r.m.s.[d] deviation bond lengths (Å)	0.011
r.m.s. deviation bond angles (degrees)	1.91

[a] $R_{sym} = \Sigma_{hkl}\Sigma_i|I_i(hkl) - I(hkl)|/\Sigma_{hkl}\Sigma_i I_i(hkl)$, where $I_i(hkl)$ and $I(hkl)$ are the ith and mean measurements of the intensity of reflection hkl.
[b] $R_{cryst} = \Sigma_{hkl}||F_o| - k|F_c||/\Sigma_{hkl}|F_o|$, where F_o and F_c are the observed and calculated structure factors for the reflection hkl, and k is a weighting factor.
[c] $R_{free} = \Sigma_{hkl}\subset_T||F_o| - k|F_c||/\Sigma_{hkl}\subset_T|F_o|$, where F_o and F_c are the observed and calculated structure factors for the reflection hkl and k is a weighing factor. T is the test set of reflections.
[d] r.m.s., root mean square.

Crystallization of QFR FrdA T234A—QFR FrdA T234A crystals were grown from protein purified by previously described methods for wild type enzyme (37) using the hanging drop vapor diffusion method in 10% polyethylene glycol 5000 monomethyl ether, 250 mM magnesium acetate, 100 mM citric acid, pH 5.8, and 0.1 mM EDTA at 22 °C with drop sizes of 1 μl. QFR crystals formed in the orthorhombic space group $P2_12_12_1$ with unit cell dimensions $a = 96.9$ Å, $b = 135.5$ Å, and $c = 266.0$ Å with $\alpha = \beta = \gamma = 90°$ (Table 1).

Data Collection, Processing, and Model Refinement—Data were collected at beamline 11-1 at the Stanford Synchrotron Radiation Laboratories on crystals cryoprotected with 30% ethylene glycol using a wavelength of 1 Å on an ADSC detector at 100 K. Data were processed using DENZO, SCALEPACK (38), and the CCP4 (39) suite of programs. Since crystals were isomorphous with crystals from known structures of wild type QFR, rigid body refinement was performed with CNS (40) to obtain initial model phases. Maps were calculated with CCP4 (39), CNS (40), and PHENIX (41). Iterative rounds of model rebuilding were performed in O (42) and COOT (43), whereas refinement was performed with CNS (40) and PHENIX (41) with loose non crystallographic symmetry restraints.

Model building with omit maps was used to minimize map bias. *Ab initio* protein folding was performed with RAPPER

TABLE 2

Kinetic parameters of wild type and mutant QFR

All assays were done at 30 °C. Fumarate reduction with methyl viologen (pH 7.0) and succinate oxidation with potassium ferricyanide (pH 8.0) were performed as described under "Experimental Procedures." ND, not determined.

	Fumarate reduction		Succinate oxidation		
	k_{cat}	K_m^{fum}	k_{cat}	K_m^{succ}	K_i^{OAA}
	s^{-1}	mM	s^{-1}	mM	μM
WT-QFR	340	0.02	30	0.55	0.3
AcT-QFR	0.4	0.8	<0.03	ND	ND
HingeT-QFR	26	0.6	1.3	2.7	40

(44). Final *R*-factors for the structures were $R_{cryst} = 26.05\%$ and $R_{free} = 29.57\%$ with reasonable geometry. Figures were created in the program PyMOL (45). The Dyndom server (39) was used to calculate the angle of domain motions between wild type QFR and hinge-T QFR.

RESULTS

In this study, two conserved threonine residues have been mutated to alanine in QFR and SQR. The first of these, act-T (Thr-A244 in QFR; Thr-A254 in SQR), hydrogen-bonds to dicarboxylate substrates bound at the active site (10, 16, 18, 21, 23). The second conserved threonine residue studied, hinge-T (Thr-A234 in QFR; Thr-A244 in SQR) hydrogen-bonds to Arg-A248 in the proton shuttle and is at the hinge region connecting the capping and FAD domains.

Active Site Threonine Mutants—Wild type SQR oxidizes succinate with a high k_{cat} of 110 s^{-1} (36); however, the SQR act-T mutant was incapable of succinate oxidation in the pH range of 6.0–9.0 tested. Moreover, heme b reduction was not observed upon prolonged incubation of the SQR act-T mutant with succinate, although wild type SQR heme b would be fully reduced under such conditions (data not shown). Similar to the SQR act-T mutant, the QFR act-T mutant (Thr-A244 → Ala) was unable to oxidize succinate. Fumarate reductase activity in the QFR act-T mutant fell by more than 800-fold compared with wild type (Table 2). The residual activity depended upon fumarate concentration, with the K_m^{fum} being increased by 40-fold (Table 2). Thus, the QFR act-T mutation affected both k_{cat} and K_m.

Since the SQR act-T mutant was catalytically inactive, the ligand binding properties of the variant enzyme were examined by optical spectroscopy. In the complex II enzyme family, hydride transfer occurs with orbital overlap between the flavin isoalloxazine N5 and the C2 of the substrate (2, 12, 26, 27). Charge transfer (CT) complexes with flavins act as intermediates in enzyme catalysis (46). In complex II enzymes, typical long wavelength absorption bands attributed to CT interaction are observed with the dicarboxylate oxaloacetate (OAA), where the partial negative charge on the C2 oxygen of OAA contributes to CT formation with oxidized flavin (17, 46). The CT formation is consistent with the OAA molecule in the active site in its tautomeric enol- or malate-like forms (10, 17, 47). Because the energy and/or intensity of CT is expected to be dependent on the orientation of the donor-acceptor partners in the complex (46, 48), this orientation can be affected by mutations. Other dicarboxylates, such as malonate and fumarate, also produce optical changes in oxidized complex II proteins but without the long wavelength CT band (17, 46). In oxidized wild type QFR and SQR, malonate and fumarate induce absorbance changes in the 350–530 nm range (Fig. 2). Enhanced absorbance at ~400 and 500 nm and decreased absorbance near 450 nm are characteristic for most dicarboxylate ligands.

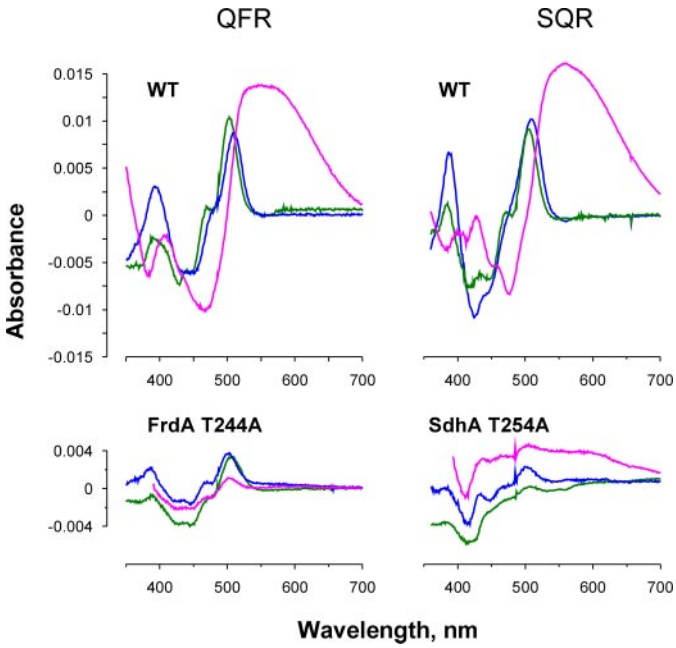

FIGURE 2. **Dicarboxylate-induced optical changes in SQR and QFR enzymes (pH 7.0, 25 °C).** Difference spectra represent the effect of malonate (*green*), fumarate (*blue*), and OAA (*magenta*) on the spectrum of fully oxidized enzymes. Dicarboxylates were used at saturating concentrations for optical spectra. For the wild type (*WT*) SQR and QFR, the concentrations of ligands were 0.1 mM OAA, 1 mM malonate, 5 mM fumarate. For the SQR act-T and QFR act-T enzymes, the concentrations were 2 mM OAA, 10 mM malonate, 10 mM fumarate. The protein concentration in all cases was normalized to 4.9 μM for spectral analysis. Shown in the figure are representative spectra of four independent experiments.

The act-T substitution resulted in dramatic changes in the ligand-induced optical properties of act-T-QFR and act-T-SQR (Fig. 2). The amplitude of the spectral peaks at 400 and 500 nm are reduced 3–4-fold in the mutant enzymes, and there is a loss of the characteristic charge transfer band in the presence of OAA (Fig. 2). These results are consistent with the observation that altered substrate binding prevents formation of the charge transfer complex and that both the QFR act-T and SQR act-T mutant enzymes are compromised in substrate binding (Table 2). This altered binding would preclude efficient catalysis.

Hinge-threonine Mutants—The next region targeted for mutagenesis was the conserved Thr in the His-Pro-Thr (HPT) sequence of QFR and SQR, since this hinge-T interacts with the proton-shuttling residue Arg-A248. The QFR hinge-T mutant showed expression levels similar to those of wild type QFR; however, the SQR hinge-T mutant was expressed at 5–7-fold lower levels than wild type (data not shown). The SQR hinge-T mutant lost succinate-ubiquinone reductase activity and heme b activity. Attempts to purify the SQR hinge-T mutant enzyme resulted in proteolysis, which was probably due to impaired stability and/or assembly of the mutant enzyme.

In contrast, the QFR hinge-T mutant was amenable to enzymatic and structural analyses over a wide pH range. The

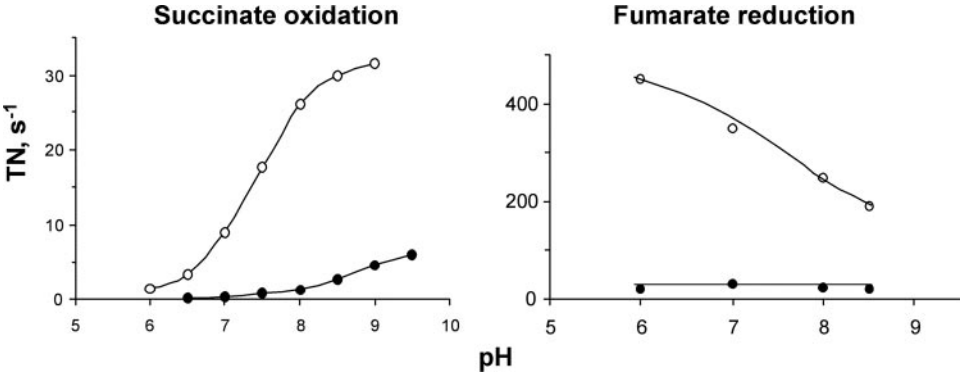

FIGURE 3. **pH dependence of succinate oxidase and fumarate reductase reactions catalyzed by wild type and hinge-T QFR enzymes (30 °C).** Enzymatic activities of wild type QFR (*open circles*) and hinge-T (FrdA T234A; *filled circles*) were performed as described under "Experimental Procedures." *TN*, turnover number.

hinge-T substitution significantly affected dicarboxylate binding at the active site (Table 2). The K_m values for fumarate and succinate significantly increased, and the K_i for OAA increased by more than 100-fold (Table 2). Typical for complex II enzymes, the pH profile of k_{cat} demonstrates a mirror-like profile, where succinate oxidation increases and fumarate reduction decreases at high pH values (49). The QFR hinge-T mutation shifted the succinate oxidation pK_a shift from 7.4 for wild type QFR to 8.7 in the mutant (Fig. 3). In the mutant, the fumarate reductase reaction is pH-independent over the pH range 6.0–8.5, consistent with the increase in apparent pK_a to over pH 8.5 (Fig. 3). Although overall catalytic activity is impaired in the QFR hinge-T mutant, the residual succinate oxidase activity at pH 9.0 is about 10% of wild type, and the fumarate reductase activity at pH 8.0 is also 10% of wild type QFR.

In agreement with the kinetic data, ligand induced optical changes in the QFR hinge-T enzyme (Fig. 4*A*). At pH 7.0, all three dicarboxylates examined induced similar spectral changes, and OAA clearly showed two spectral features. One was a peak at 500 nm characteristic of the other dicarboxylates. The second change was a significantly reduced charge transfer band (500–700 nm) compared with wild type QFR (Fig. 2), consistent with a change of relative orientation of the OAA and flavin in the mutant at pH 7.0 (48). At pH 9.0, where the hinge-T mutant demonstrated 10-fold higher activity than at pH 7.0, the increased absorbance of the charge transfer band closely resembled that seen for wild type QFR. The OAA-induced optical changes for wild type QFR did not significantly differ between pH 7.0 and 9.0 (Fig. 4*C*).

Structural Characterization of the QFR Hinge-T Mutant—To provide a structural framework for how the hinge-T substitution affected substrate binding and enzyme activity, the structure was determined to 3.65 Å resolution using x-ray crystallography. Previous *E. coli* QFR structures show clear electron density for the weak inhibitor citrate bound at the active site, due to citrate in the crystallization conditions (23, 50). The QFR hinge-T mutation caused a dramatically decreased affinity for dicarboxylate inhibitors (Table 2), and despite the presence of 100 mM citrate in the crystallization reaction, the structure of the mutant enzyme showed no clear electron density in the active site.

Loss of substrate binding in the hinge-T mutant may be explained upon examination of the structure. In homologue structures where the capping domain and FAD domain are in a closed conformation (21, 23, 50), a minimum of one-third of the hydrogen bonds to substrate are provided by residues of the capping domain. In the QFR hinge-T structure, the capping domain rotated by 5.3°, opening a pathway to the active site (Fig. 5*A*). The new rotated capping domain position resembles the maximally open conformation observed in the *Shewanella* Fcc_3 enzyme (9). This rotation moves the capping domain side chains into positions where they no longer hydrogen-bond to substrate or inhibitors. Consistent with this, all structures to date with an open position of the capping domain lack bound substrate at the active site.

Particularly important to catalytic activity are Arg-A287, the proton donor during reduction, and Thr-A244, which is critical for transition state formation. In the majority of crystal structures of complex II homologs, the guanidino group of the residue equivalent to Arg-A287 is poised for proton transfer to substrate, since it forms a hydrogen bond to the bound dicarboxylate (10, 11, 19, 20, 22). In the hinge-T mutant, the movement of the capping domain into the open position shifted the Cα atom of Arg A287 5.5 Å from the active site and moved the Nζ atom of the side chain to a distance too far for proton transfer. The act-T side chain was also located on the capping domain. In the hinge-T mutant, the domain rotation moved the Cα atom of act-T by 1.5 Å and shifted the side chain away from the dicarboxylate binding site. The repositioning of both Arg-A287 and act-T may contribute to the observed decrease in the reaction rate in the hinge-T mutant.

In the hinge-T mutant, the rotation of the capping domain into the open conformation was associated with decreased electron density quality compared with other regions of the mutant QFR. This was shown by an increase in crystallographic temperature factors. In the structure, the average temperature factor was 72 Å^2 in the FAD-binding domain main chain as compared with 168 Å^2 in the capping domain main chain. A similar temperature factor increase is observed in the *Shewanella* Fcc_3 open conformation structure (Protein Data Bank code 1QO8) (9). The electron density maps for the hinge-T mutation lacked appreciable density for many of the side chains. Nevertheless, it is clear that the domain rotation observed in the hinge-T mutation results in alterations of the hydrogen bond network of Arg-A287 and Arg-A248 in the proton shuttle, which may alter the pK_a values of each side chain. In addition to the 5.5-Å shift of Arg-A287, the Cα atom of Arg-A248 shifted 2.1 Å away from the active site (Fig. 5*B*). As described above, the hinge-T mutant had an altered pH profile as compared with wild type. The hinge-T Oγ–Arg-A248 Nζ hydrogen bond probably serves to modulate the pK_a of Arg-A248 so that loss of the hydrogen bond from the Oγ of Thr-A234 to the guanidino group of Arg-A248 may raise the pK_a of the Arg-A248 side chain. Crystallographic electron density does not unambiguously reveal the

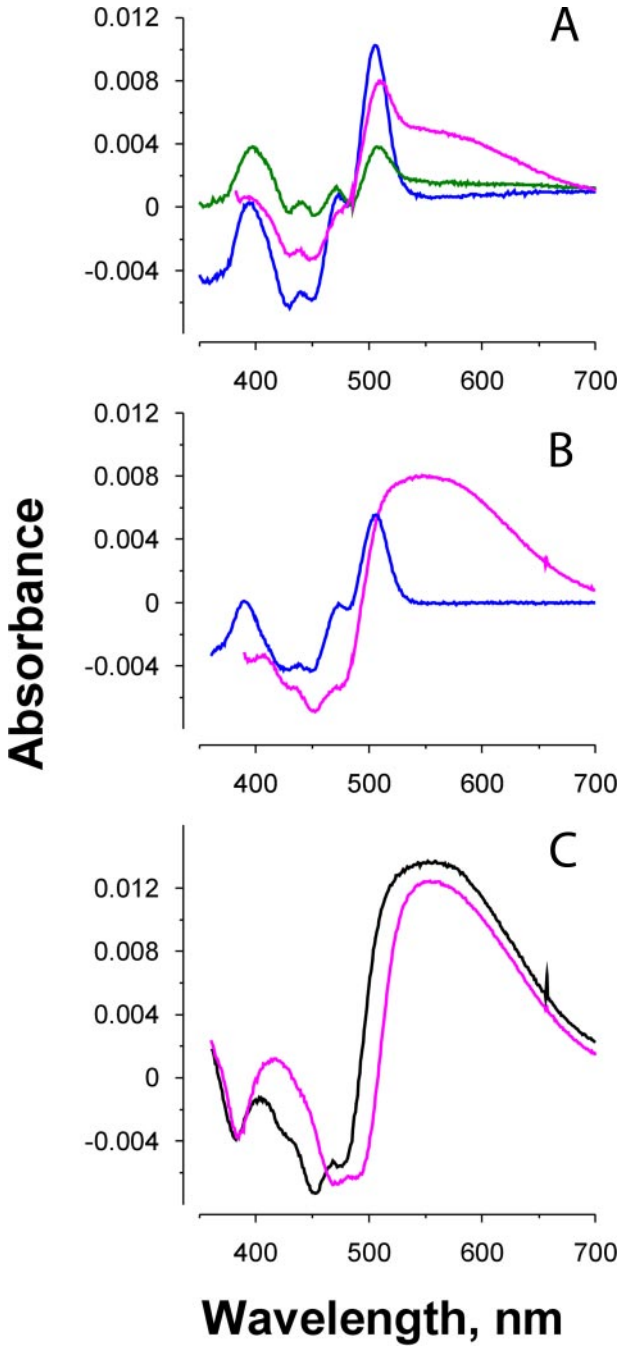

FIGURE 4. **Ligand-induced optical changes of hinge-T QFR enzyme (25 °C).** *A* and *B*, difference spectra show the effect of malonate (*green*; 10 mM) fumarate (*blue*; 10 mM), and OAA (*magenta*; 2 mM) on the spectrum of fully oxidized FrdA T234A enzymes at pH 7.0 (*A*) and 9.0 (*B*). The concentrations of ligands were 10 mM malonate, 10 mM fumarate, and 2 mM OAA. *C*, OAA induced spectral changes of wild type QFR at pH 7.0 (*black*) and 9.0 (*magenta*). Protein concentration of wild type and hinge-T QFR was 4.9 μM.

Arg-A248 side chain position, which is most likely disordered and solvent-exposed.

DISCUSSION

The *E. coli* complex II homologs QFR and SQR contain covalently bound FAD and thus are able to reversibly oxidize succinate or reduce fumarate (49). This makes them useful models for study of bidirectional catalysis in complex II enzymes (1, 12, 49). An active site loop identified between act-T (QFR Thr-A244; SQR Thr-A254) and hinge-T (QFR Thr-A234; SQR Thr-A244) was tested for its importance in catalysis of the reaction in both directions for two reasons; first, it provides numerous hydrogen bonds to substrate, and second, it provides a key stabilizing interaction with the proton shuttle. In this study, the role of the two conserved threonine residues in this loop was investigated.

The Act-T Hydrogen Bond May Stabilize the Transition State—Structures of Fcc_3 fumarate reductases and the *W. succinogenes* QFR co-crystallized with fumarate show a twisted conformation of the C1 carboxylate in the species bound at the active site. Fumarate twisting may strain the double bond and decrease the free energy barrier for attaining the transition state (11, 12, 21). Elimination of the act-T side chain, which hydrogen-bonds to the carbonyl where fumarate is twisted, dramatically impairs catalysis of both the *E. coli* SQR and QFR enzymes (Table 2). The altered binding of dicarboxylate ligands in the act-T mutant is seen with the absence of CT absorbance upon OAA binding and significantly decreased spectral changes upon fumarate or malonate binding (Fig. 2). This suggests that the removal of the act-T Oγ hydrogen bond affects both substrate binding and transition state stabilization. In contrast, substitutions of other active site residues equivalent to *E. coli* FrdA His-232 and His-354 were mainly shown to affect substrate binding (12, 26, 51).

Furthermore, in the Fcc_3 enzyme, x-ray crystallography of a mutant enzyme equivalent to *E. coli* QFR FrdA H232A only showed subtle changes in the position of fumarate; however, the C1 carboxyl group is found in the same twisted conformation as in wild type enzyme (26), indicating that this histidine does not participate in transition state formation. The substitution of the active site threonine (FrdA Thr-244/SdhA Thr-254) to alanine caused a much more dramatic effect on complex II enzyme activity compared with the single substitutions of the two histidine residues found at the active site in the soluble Fcc_3 enzyme (26). The results presented here are consistent with act-T being essential for positioning the C1 carboxyl of fumarate and efficient catalysis in the complex II family of enzymes.

The Hinge-T Mutant May Trap the Proton Shuttle in an Intermediate State—Hinge-T (Thr-A234 in QFR; Thr-A244 in SQR) in the conserved His-Pro-Thr of the capping domain hydrogen-bonds to the Arg-A248 side chain, part of the complex II proton shuttle. The effect of removing this hydrogen-bonding interaction was investigated. The hinge-T variant enzyme demonstrates altered pH dependence of the catalyzed reactions. This has several plausible explanations that are not mutually exclusive. First, the elimination of the hydrogen bond from Thr-A234 to Arg-A248 may alter the Arg-A248 side chain conformation so that it no longer can transfer protons to Glu-A245, thereby disrupting catalytic activity. Since electron density for the side chain of Arg-A248 could not be observed in the hinge-T mutant structure, the orientation of Arg-A248 in the hinge-T variant cannot be unambiguously established. A second explanation is that the loss of a hydrogen bond to Arg-A248 may shift the pK_a of the proton shuttle. This may correlate with the increased succinate oxidase activity and stabilization of the OAA anionic transition state at high pH. In wild type QFR, the

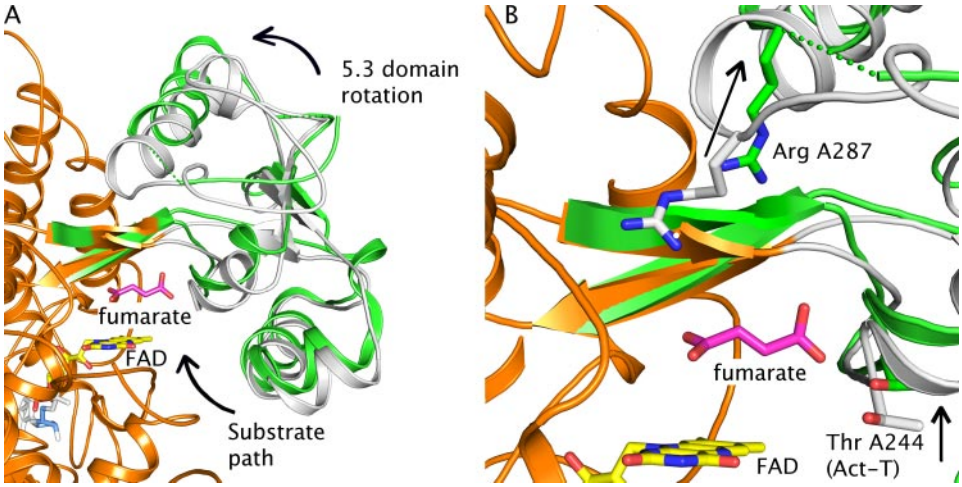

FIGURE 5. **Comparison of the position of the capping domain in wild type and hinge-T (FrdA T234A) QFR.** The hinge-T QFR capping domain (*green*) is superimposed onto the flavoprotein of wild type QFR capping domain (*gray*). *Green dashes* connect the main chain of the hinge-T mutant in regions where the crystallographic electron density does not allow the main chain to be resolved unambiguously. Side chain carbons are colored *gray* in wild type QFR and are colored *green* in the hinge-T mutant. FAD carbons are colored *yellow*, nitrogen atoms are colored *blue*, and oxygen is colored *red*. *A*, In the hinge-T mutant, the structure of the FAD-binding domain (*orange*) is not significantly altered and can be superimposed with a root mean square deviation of 0.3 Å. However, the capping domain has rotated 5.3° with respect to the wild type enzyme (Protein Data Bank code 1KF6). The direction of the capping domain rotation and the proposed substrate path are denoted with *black arrows*. *B*, the altered position of the capping domain shifts the proton shuttling residues in the hinge-T mutant. The *black arrows* indicate the direction of local structural changes.

CT amplitude does not change at pH 7 or 9 and does not correlate with the pK_a of the reaction (36, 49). This suggests that microscopic pK_a values of amino acid residues involved in substrate activation are below pH 7, and the observed pK_a of the reaction is influenced by other active site or proton shuttle residues. Increased stabilization of the CT species in the hinge-T mutant with increased pH may reflect either change in the pK_a of the residues involved in substrate activation *or* conformational changes in the movable capping domain that effect ionization properties of the active site residues and/or substrate binding position.

Proton Shuttle Regeneration May Trigger Domain Movements during Catalysis—Unexpectedly, a dramatically decreased substrate affinity is observed in the hinge-T mutant enzyme. The x-ray structure of the hinge-T variant reveals a rearrangement between the FAD-binding and capping domains of the flavoprotein subunit that disrupts hydrogen bonding to substrate and prevents optimal substrate orientation for catalysis. Sequence and structural analysis support the possibility that the orientation between the capping domain and FAD-binding domain is not fixed. The capping domain contains a disproportionate number of glycine residues. Of the 120 residues in the capping domain, 19 are glycines, and of those, seven are within the first 20 residues of the capping domain. Glycines typically predominate where their added flexibility allows conformational rearrangements of proteins.

The interdomain angles appear to be influenced by the presence of substrate at the active site. In the higher resolution Fcc_3 structures (11), which allow for reliable identification of hydrogen bonds, only 11 interdomain hydrogen bonds between the FAD domain and the capping domain stabilize the closed state. Of these, six are between the polypeptide chains, and five are to substrate. Consequently, lack of bound substrate would probably destabilize a closed conformation. Similarly, the wild type *E. coli* QFR structure was determined in complex with citrate in an intermediate position of the FAD-binding and capping domains (50). In the intermediate structure, a decreased percentage of stabilizing hydrogen-bonding interactions are observed; only eight hydrogen bonds mediate this contact. In this case, it is the hydrogen bonds to the dicarboxylate that are exclusively lost, such that in the intermediate position of the capping domain, only two through-substrate bonds remain. Furthermore, all open structures of flavoprotein homologues, including this new structure of the hinge-T mutant, lack crystallographic electron density corresponding to bound dicarboxylate at the active site.

In previous structures, it was unclear how crystal contacts influenced domain opening. This hinge-T mutant has the same crystal packing as wild type and exhibits a domain rotation, indicating that the rotation is probably correlated to the enzymatic state and not an artifact of different crystallization conditions. The low number of stabilizing contacts, a high percentage of which are through substrate, suggests that the kinetic barrier between open and closed states is low and can be influenced by substrate binding. As a result, substrate binding or proton shuttle state could heavily influence the conformation. Flavoproteins in general may use such movements to control active site solvation as a means of optimizing catalysis and even determining the enzyme's role as an oxidase, oxygenase, or dehydrogenase (25, 52).

The possibility that domain reorientation accompanies catalysis and may correlate with the proton shuttle state stands in contrast to previous studies in a soluble QFR homolog (Fcc_3) from *Shewanella frigidimarina*, which suggest a minimal role for capping domain mobility in fumarate catalysis (24). There, a disulfide bond was introduced between the capping domain and the rest of the flavoprotein to restrict capping domain movement. This disulfide bond reduced catalysis by 90%, and it was argued that this constituted an insignificant decrease in activity. One possible explanation for the difference in models from Fcc_3 and the QFR hinge-T mutant could be due to the nature of soluble fumarate reductases compared with membrane-bound complex II homologs. In all structures of the *E. coli* QFR determined to date, the electron density maps showed significantly better quality for integral membrane polypeptides than for the soluble domain.[4] Thus, it is possible that membrane association may add sta-

[4] T. M. Iverson, unpublished observation.

bility to the entire protein and allow for conformational freedom in the soluble domain in *E. coli* QFR. Furthermore, other capping domain movements may compensate for the motion restriction imposed by the disulfide bond, allowing the substrate access to the active site.

Act-T May Work in Concert with Domain Movements to Promote the Formation of the Transition State—Although there are several possibilities for the observed domain reorientations in the hinge-T mutant, the design of this variant to mimic a regenerating proton shuttle suggest that this movement accompanies catalysis. As seen in Fig. S1 (movie), a channel that forms in the ligand-free conformation allows substrate to access the active site. The open orientation of the two domains poises the act-T side chain to form essential hydrogen-bonding interactions that selectively pull the substrate into the active site. Subsequently, the bonds between act-T and substrate may induce active site closure by rotation of the capping domain to form further hydrogen bonding interactions with the substrate. Domain closure may force the interaction between act-T and substrate to twist the C1 carboxyl group and strain the double bond of fumarate while concomitantly orienting the proton shuttle Arg-A287 into an optimal position for catalysis. In this now solvent-protected active site, the dicarboxylate transition state can accept hydride from FAD and a proton from Arg-A287.

Conclusions—The roles of two threonine residues on an active site loop were analyzed with the mutation to alanine. The act-T mutation shows the importance of a hydrogen bond to substrate that stabilizes the high energy intermediate states. Movement of the active site loop and the capping domain from open to closed states may serve to twist the substrate into a transition state for catalysis. Fluctuation between the open and closed states of the capping domain may protect the high energy intermediate from water in the active site while still permitting substrate binding in the open state. This may serve as an important mechanism to enhance on-pathway catalytic efficiency while minimizing the formation of off-pathway side products.

Acknowledgments—We thank Eric Dawson for helpful discussions, Yelizaveta Sher and Violetta Kotlyar for construction of site-directed mutations, and Anne Karpay for assistance with data collection. Diffraction data were collected at the Stanford Synchrotron Radiation Laboratories, which is operated by the United States Department of Energy.

REFERENCES

1. Cecchini, G. (2003) *Annu. Rev. Biochem.* **72,** 77–109
2. Iverson, T. M., Luna-Chavez, C., Schröder, I., Cecchini, G., and Rees, D. C. (2000) *Curr. Opin. Struct. Biol.* **10,** 448–455
3. Ohnishi, T., King, T. E., Salerno, J. C., Blum, H., Bowyer, J. R., and Maida, T. (1981) *J. Biol. Chem.* **256,** 5577–5582
4. Blaut, M., Whittaker, K., Valdovinos, A., Ackrell, B. A. C., Gunsalus, R. P., and Cecchini, G. (1989) *J. Biol. Chem.* **264,** 13599–13604
5. Ackrell, B. A. C., Cochran, B., and Cecchini, G. (1989) *Arch. Biochem. Biophys.* **268,** 26–34
6. Leger, C., Heffron, K., Pershad, H. R., Maklashina, E., Luna-Chavez, C., Cecchini, G., Ackrell, B. A. C., and Armstrong, F. A. (2001) *Biochemistry* **40,** 11234–11245
7. Jeuken, L. J. C., Jones, A. K., Chapman, S. K., Cecchini, G., and Armstrong, F. A. (2002) *J. Amer. Chem. Soc.* **124,** 5702–5713
8. Mattevi, A., Tedeschi, G., Bacchella, L., Coda, A., Negri, A., and Ronchi, S. (1999) *Structure* **7,** 745–756
9. Bamford, V., Dobbin, P. S., Richardson, D. J., and Hemmings, A. M. (1999) *Nat. Struct. Biol.* **6,** 1104–1107
10. Taylor, P., Pealing, S. L., Reid, G. A., Chapman, S. K., and Walkinshaw, M. D. (1999) *Nat. Struct. Biol.* **6,** 1108–1112
11. Leys, D., Tsapin, A. S., Nealson, K. H., Meyer, T. E., Cusanovich, M. A., and Van Beeumen, J. J. (1999) *Nat. Struct. Biol.* **6,** 1113–1117
12. Reid, G. A., Miles, C. S., Moysey, R. K., Pankhurst, K. L., and Chapman, S. K. (2000) *Biochim. Biophys. Acta* **1459,** 310–315
13. Lancaster, C. R. D. (2003) *Adv. Protein Chem.* **63,** 131–149
14. Ackrell, B. A. C. (2000) *FEBS Lett.* **466,** 1–5
15. Lancaster, C. R. D., and Kroger, A. (2000) *Biochim. Biophys. Acta* **1459,** 422–431
16. Sun, F., Huo, X., Zhai, Y., Wang, A., Xu, J., Su, D., Bartlam, M., and Rao, Z. (2005) *Cell* **121,** 1043–1057
17. Huang, L. S., Shen, J. T., Wang, A. C., and Berry, E. A. (2006) *Biochim. Biophys. Acta* **1757,** 1073–1083
18. Yankovskaya, V., Horsefield, R., Törnroth, S., Luna-Chavez, C., Miyoshi, H., Léger, C., Byrne, B., Cecchini, G., and Iwata, S. (2003) *Science* **299,** 700–704
19. Huang, L. S., Sun, G., Cobessi, D., Wang, A. C., Shen, J. T., Tung, E. Y., Anderson, V. E., and Berry, E. A. (2006) *J. Biol. Chem.* **281,** 5965–5972
20. Madej, M. G., Nasiri, H. R., Hilgendorff, N. S., Schwalbe, H., and Lancaster, C. R. D. (2006) *EMBO J.* **25,** 4963–4970
21. Lancaster, C. R. D., Kroger, A., Auer, M., and Michel, H. (1999) *Nature* **402,** 377–385
22. Lancaster, C. R. D., Gross, R., and Simon, J. (2001) *Eur. J. Biochem.* **268,** 1820–1827
23. Iverson, T. M., Luna-Chavez, C., Cecchini, G., and Rees, D. C. (1999) *Science* **284,** 1961–1966
24. Rothery, E. L., Mowat, C. G., Miles, C. S., Mott, S., Walkinshaw, M. D., Reid, G. A., and Chapman, S. K. (2004) *Biochemistry* **43,** 4983–4989
25. Mattevi, A. (2006) *Trends Biochem. Sci.* **31,** 276–283
26. Doherty, M. K., Pealing, S. L., Miles, C. S., Moysey, R., Taylor, P., Walkinshaw, M. D., Reid, G. A., and Chapman, S. K. (2000) *Biochemistry* **39,** 10695–10701
27. Pankhurst, K. L., Mowat, C. G., Miles, C. S., Leys, D., Walkinshaw, M. D., Reid, G. A., and Chapman, S. K. (2002) *Biochemistry* **41,** 8551–8556
28. Mowat, C. G., Moysey, R., Miles, C. S., Leys, D., Doherty, M. K., Taylor, P., Walkinshaw, M. D., Reid, G. A., and Chapman, S. K. (2001) *Biochemistry* **40,** 12292–12298
29. Pankhurst, K. L., Mowat, C. G., Rothery, E. L., Hudson, J. M., Jones, A. K., Miles, C. S., Walkinshaw, M. D., Armstrong, F. A., Reid, G. A., and Chapman, S. K. (2006) *J. Biol. Chem.* **281,** 20589–20597
30. Westenberg, D. J., Gunsalus, R. P., Ackrell, B. A. C., Sices, H., and Cecchini, G. (1993) *J. Biol. Chem.* **268,** 815–822
31. Maklashina, E., Berthold, D. A., and Cecchini, G. (1998) *J. Bacteriol.* **180,** 5989–5996
32. Maklashina, E., Rothery, R. A., Weiner, J. H., and Cecchini, G. (2001) *J. Biol. Chem.* **276,** 18968–18976
33. Rothery, R. A., Seime, A. M., Spiers, A. M. C., Maklashina, E., Schroder, I., Gunsalus, R. P., Cecchini, G., and Weiner, J. H. (2005) *FEBS J.* **272,** 313–326
34. Kita, K., Vibat, C. R. T., Meinhardt, S., Guest, J. R., and Gennis, R. B. (1989) *J. Biol. Chem.* **264,** 2672–2677
35. Maklashina, E., Hellwig, P., Rothery, R. A., Kotlyar, V., Sher, Y., Weiner, J. H., and Cecchini, G. (2006) *J. Biol. Chem.* **281,** 26655–26664
36. Maklashina, E., Iverson, T. M., Sher, Y., Kotlyar, V., Andréll, J., Mirza, O., Hudson, J. M., Armstrong, F. A., Rothery, R. A., Weiner, J. H., and Cecchini, G. (2006) *J. Biol. Chem.* **281,** 11357–11365
37. Luna-Chavez, C., Iverson, T. M., Rees, D. C., and Cecchini, G. (2000). *Protein Expression Purif.* **19,** 188–196
38. Otwinowski, Z. (1993) in *CCP4 Study Weekend Data Collection and Processing* (Sawyer, L., Isaacs, N., and Bailey S., eds) pp. 56–62, SERC Daresbury Laboratory, United Kingdom

39. Bailey, S. (1994) *Acta Crystallogr. Sect. D* **50,** 760–763
40. Brunger, A. T., Adams, P. D., Clore, G. M., DeLano, W. L., Gros, P., Grosse-Kunstleve, R. W., Jiang, J. S., Kuszewski, J., Nilges, M., Pannu, N. S., Read, R. J., Rice, L. M., Simonson, T., and Warren, G. L. (1998) *Acta Crystallogr. Sect. D* **54,** 905–921
41. Adams, P. D., Grosse-Kunstleve, R. W., Hung, L. W., Ioerger, T. R., McCoy, A. J., Moriarty, N. W., Read, R. J., Sacchettini, J. C., Sauter, N. K., and Terwilliger, T. C. (2002) *Acta Crystallogr. Sect. D* **58,** 1948–1954
42. Jones, T. A., Zou, J. Y., Cowan, S. W., and Kjeldgaard, M. (1991) *Acta Crystallogr. Sect. A* **47,** 110–119
43. Emsley, P., and Cowtan, K. (2004) *Acta Crystallogr. Sect. D* **60,** 2126–2132
44. DePristo, M. A., de Bakker, P. I. W., Johnson, R. J. K., and Blundell, T. L. (2005) *Structure* **13,** 1311–1319
45. DeLano, W. L. (2002) *PyMOL*, DeLano Scientific, Palo Alto, CA
46. Veeger, C., Dervartanian, D. V., Kalse, J. F., de Kok, A., and Koster, J. F. (1966) in *Flavins and Flavoproteins* (Slater, E. C., ed) pp. 242–262, Elsevier, Amsterdam, The Netherlands
47. Wardrope, C., Mowat, C. G., Walkinshaw, M. D., Reid, G. A., and Chapman, S. K. (2006) *FEBS Lett.* **580,** 1677–1680
48. Massey, V., and Ghisla, S. (1974) *Ann. N. Y. Acad. Sci.* **227,** 446–465
49. Maklashina, E., and Cecchini, G. (1999) *Arch. Biochem. Biophys.* **369,** 223–232
50. Iverson, T. M., Luna-Chavez, C., Croal, L. R., Cecchini, G., and Rees, D. C. (2002) *J. Biol. Chem.* **277,** 16124–16130
51. Schröder, I., Gunsalus, R. P., Ackrell, B. A. C., Cochran, B., and Cecchini, G. (1991) *J. Biol. Chem.* **266,** 13572–13579
52. Bossi, R. T., Negri, A., Tedeschi, G., and Mattevi, A. (2002) *Biochemistry* **41,** 3018–3024